12 W high power InGaAsP/AlGaInP 755 nm quantum well laser

H. Martin Hu (胡 海)[1,2], Jianyang Zhao (赵健阳)[3], Weimin Wang (汪卫敏)[3], James Ho (何晋国)[1,2], Langxing Kuang (邝朗醒)[3], and Wenbin Liu (刘文斌)[3,*]

[1]*Research Institute of Tsinghua University in Shenzhen, Shenzhen 518057, China*
[2]*Guangdong Provincial Key Laboratory of Optomechatronics, Shenzhen 518057, China*
[3]*Shenzhen Raybow Optoelectronics Co., Ltd., Shenzhen 518055, China*
**Corresponding author: liuwenbin@raybowlaser.com*

Received January 21, 2019; accepted March 14, 2019; posted online June 4, 2019

High power laser diodes (LDs) with a lasing wavelength between 700 and 780 nm have great potential in various medical uses. Here, we report our recent efforts in developing an InGaAsP/AlGaInP-based commercial high power edge-emitting LD, which has 755 nm emission peak with a world-record continuous wave output power of 12.7 W, the highest reported so far. The lack of Al atoms in the active region significantly lowers the chance of catastrophic optical damage during high power laser operation. Meanwhile, with an accumulated 3800 h running time, our ongoing aging tests reveal excellent reliability of our devices.

OCIS codes: 140.2020, 140.5960.
doi: 10.3788/COL201917.061403.

Lasers with an emitting wavelength between 700 and 780 nm have found great potential in extensive biomedical use[1,2], for instance, cancer treatment, permanent hair removal, and measurement of hemoglobin in blood cells. Photons with different wavelengths have different penetration depths under human skin. Within the 700–780 nm wavelength range, the human tissue is relatively transparent, which allows the photons to reach deep beneath surface skin. During the operation, a laser beam is directed to a specific area and destroys the target tissue by photo-thermal heating, while leaving surrounding tissue intact. In particular, the widely used alexandrite solid-state lasers operate at 755 nm, which corresponds to an absorption peak of different chromophore in organisms that may induce various skin diseases. But, in the meantime, lasers can also be absorbed by the hemoglobin in blood, which is an undesired feature. Compared to lasers working at other wavelengths that are dedicated to medical treatment, for instance, 808 and 1064 nm, the competitive absorption from hemoglobin is the lowest at 755 nm. Laser diodes (LDs) with a spectrum peaked around 755 nm can be used to pump alexandrite lasers or even replace them when the output power is sufficiently large, and the lifetime is acceptably long.

The development of semiconductor LDs operating in this wavelength range has long been limited by materials. Traditionally, the unstrained or compressively strained (In)AlGaAs/GaAs material system is used to cover the wavelength between 730 and 780 nm[3,4], but the high power performance under high temperature is so poor as a result of weak electron confinement and increased possibility of catastrophic optical damage (COD). It has been confirmed that such shortcomings are due to the increased amount of Al introduced into the active region. To bypass the limitations imposed by the (In)AlGaAs/GaAs material system, several alternative core Al free material systems like strain tunable (In)GaAsP/AlGaAs/GaAs and (In)GaAsP/AlGaInP/GaAs have been suggested and proved to cover a wider 700–790 nm wavelength range and outperform its predecessor in high power operation[5–9].

In this Letter, we present the design and experimental data of our near infrared (NIR) edge-emitting 755 nm high power LDs based on an InGaAsP compressively strained quantum well (QW) and AlGaInP waveguide and cladding layers. The device is fabricated on a GaAs substrate, and each layer is prepared using metal organic chemical vapor deposition (MOCVD). It has a record-high 12.7 W continuous wave (CW) output power and long lifetime of over 3800 h. Compared to other LDs operating in the 730–780 nm wavelength range, it is a huge step forward[4,5,7,9]. We are confident that in the future our LDs can replace the alexandrite laser.

The key factors limiting the output power are the COD power and thermal rollover. To overcome the barrier imposed by COD, we adopt a thick waveguide layer, long cavity design, and a broad emitting width so that the power density at the facet and in the bulk is kept low. Considering the reduced device efficiency when the thermal heating is strong, AlGaInP is used instead of AlGaAs as waveguide and cladding layer material. The former provides stronger electron confinement inside the QW and is easier for fabrication[9].

As can be seen from Fig. 1, the active layer consists of a 6 nm $In_{0.4}Ga_{0.6}As_{0.34}P_{0.66}$ compressively strained single QW sandwiched between AlGaInP waveguide layers. Conventional symmetric waveguide and cladding layers are adopted to maximize the optical confinement factor in the QW so that the threshold current will not be too high.

The waveguide structure consists of two different epilayers. Since the Al composition affects the material

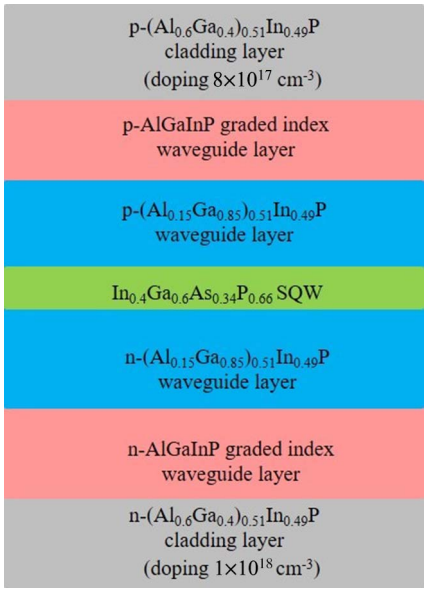

Fig. 1. Schematic epitaxial structure for product RB-755.

refractive index to a much greater degree than any other element in the AlGaInP material system, the waveguiding mechanism in the epi-growth direction is realized by easily adjusting the Al fraction in each of the waveguide layers and the outer cladding layer, which are lattice-matched to the GaAs substrate. The refractive index decreases rapidly as Al increases; thus, the inner-most waveguide layer $(Al_{0.15}Ga_{0.85})_{0.51}In_{0.49}P$ has the smallest fraction of aluminum with a thickness of 500 nm and no dopants. Outside this undoped AlGaInP layer is a 200 nm graded index waveguide structure, which consists of AlGaInP with a linear variation in the Al fraction from $(Al_{0.15}Ga_{0.85})_{0.51}In_{0.49}P$ to $(Al_{0.6}Ga_{0.4})_{0.51}In_{0.49}P$ and is undoped as well. Furthermore, the graded waveguide structure is sandwiched by a 1.2 μm outer $(Al_{0.6}Ga_{0.4})_{0.51}In_{0.49}P$ cladding layer, whose higher Al content provides optical confinement for the waveguide layers. The cladding layers are p type (doping level 8×10^{17} cm^{-3}) and n type (doping level 1×10^{18} cm^{-3}) doped in the upper and lower sections, respectively.

Based on such a structure design, calculations are done to provide some valuable information. In the $(Al_xGa_{1-x})_{1-y}In_yP$ material system, the refractive index varies approximately linearly with Al composition x. When $(Al_xGa_{1-x})_{1-y}In_yP$ layers are lattice-matched to the GaAs substrate ($y = 0.49$), the refractive index can be expressed as[10]

$$n = n_0 - 0.37 \cdot x, \tag{1}$$

where x is the composition of Al, and n_0 is the refractive index of $Ga_{0.51}In_{0.49}P$. By using such data for index differences between layers, we performed a one-dimensional (1D) beam propagation method (BPM) simulation to get the optical properties of our device in wafer growth direction. Results are presented in Fig. 2.

The epitaxial structure of our 755 nm laser was grown by MOCVD. The fabrication was performed using the routine semiconductor laser process. A shallow ridge was formed by wet-etching to remove the heavily doped p-type contact layer, and then p-metal contact was carried out, followed by the wafer thinning and n-metal contact. The emitter width is 0.35 mm, and the cavity length is 2.5 mm.The bars were cleaved and then protected by a facet passivation process. Facet coating for high reflection (HR) and anti-reflection (AR) was finally performed, with the HR reflectivity being about 98% and the AR reflectivity being 8%, respectively.

After facet coating, laser bars were screened by bar testing, where power-current-voltage (*P-I-V*), far-field, and optical spectrum data were automatically collected for every chip in a bar. Good chips were selected and diced into individual dies before being mounted onto metalized AlN submount with an AuSn hard solder process.

Various tests including *P-I-V* curves, far-field divergence, spectrum, and lifetime have been performed with chip on submount (COS) packaging form. Figure 3(a) shows *P-I-V* curves of one of our LDs under CW working

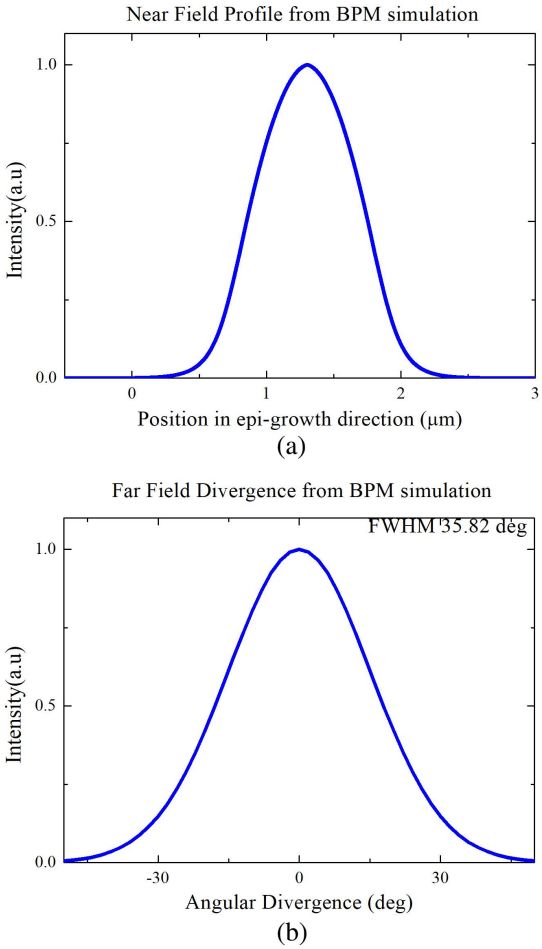

Fig. 2. (a) Calculated near-field distribution in the vertical direction, fundamental mode only. The confinement factor Γ is approximately 0.7%. (b) Calculated far-field divergence, with a full width at half maximum (FWHM) of 35.82°.

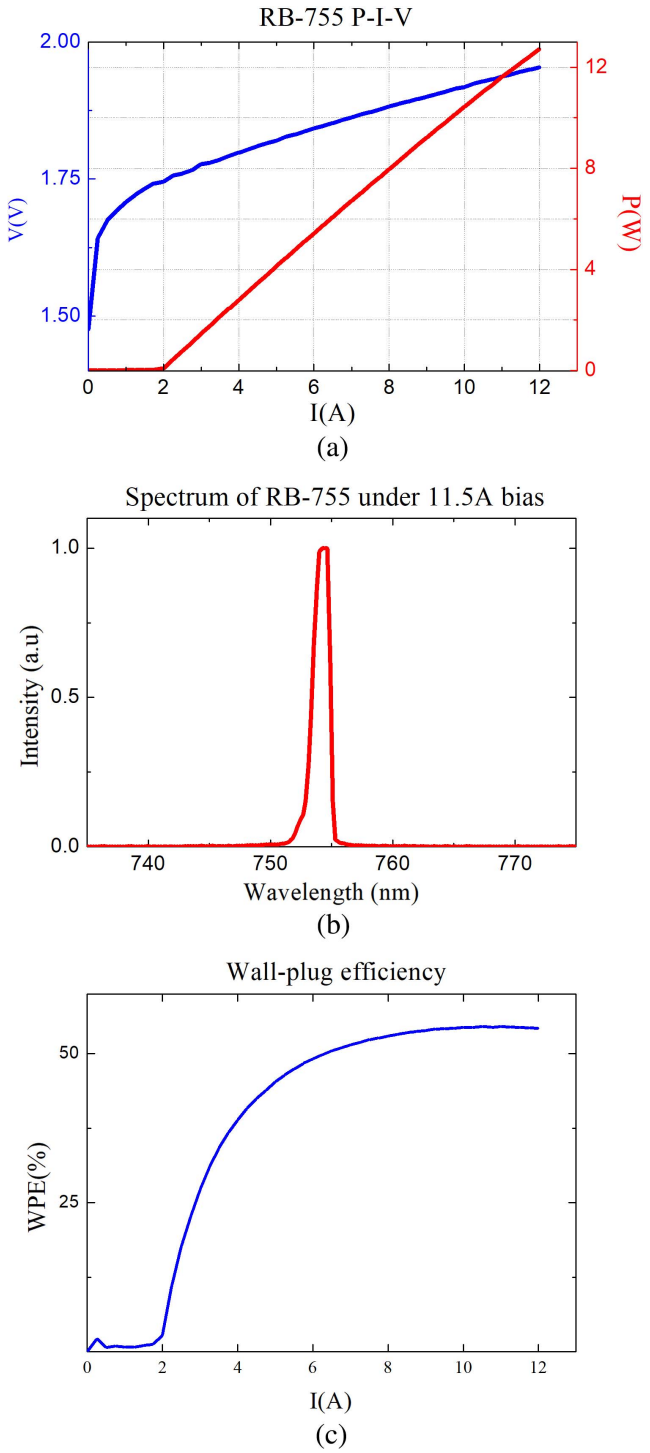

Fig. 3. (a) *P-I-V* curves of product RB-755. (b) Spectrum of a single emitter in COS packaging under 11.5 A bias and 25°C. (c) Wall-plug efficiency of RB-755.

conditions at the temperature of 25°C. The threshold current is roughly 2 A, and the slope efficiency is around 1.27 W/A. Even when the current is increased to the high value of 12 A, good linearity of the *P-I* characteristics is still preserved. The optical power reaches 12.7 W at the current of 12 A. This is the highest output power at the 755 nm wavelength from a single semiconductor LD to the best of our knowledge. The wall-plug efficiency is plotted in Fig. 3(c) as a function of the injecting current; the maximal value is 54.5%, and it is 54.4% at 12 W output power.

It is worth mentioning that catastrophic optical mirror damage (COMD) did not happen, even when the output exceeded 12 W. COMD power is found to be much higher than 15 W under quasi-CW (QCW) testing conditions. Figure 3(b) shows the spectrum of the same single emitter under 11.5 A bias when the optical power is approximately 12 W [Fig. 3(a)]. Sharp peaks centered at 754.5 nm indicate that light emitted from our LDs is highly monochromatic.

Based on such data, the lifetime test is carried out with 12 A CW injection current at a temperature of 40°C (Fig. 4). In Fig. 4, the initial power is defined as P_0 and the instant power as P. The ratio P/P_0 was constantly monitored by our equipment, and its value remained roughly one with only minor fluctuations for 3800 h until the time of writing of this Letter. Because we observed no slow degradation of the optical power during the lifetime test, thus we think the sudden failure of COD is the only failure mechanism for our laser. According to the model in the Ref. [11], we anticipate the lifetime of our 755 nm laser is more than 50,000 h at 8 W operation power.

The far-field angular divergence is measured, as in Fig. 5. The vertical far-field characteristics [Fig. 5(a)] agree well with simulated data using BPM [Fig. 2(b)]. By defining the divergence to be the full width at half maximum, the fast axis divergence is between 36° and 38° [Fig. 5(a)], and the slow axis divergence is around 7°–8° [Fig. 5(b)]. The small slow-axis divergent angle indicates that the 755 nm LDs have good brightness.

Another important feature of an LD is the characteristic temperature. The threshold current I_{th} can be defined as a function of absolute temperature T,

$$I_{\mathrm{th}}(T) = I_0 \cdot \exp\left(\frac{T - T_0}{T_0}\right), \tag{2}$$

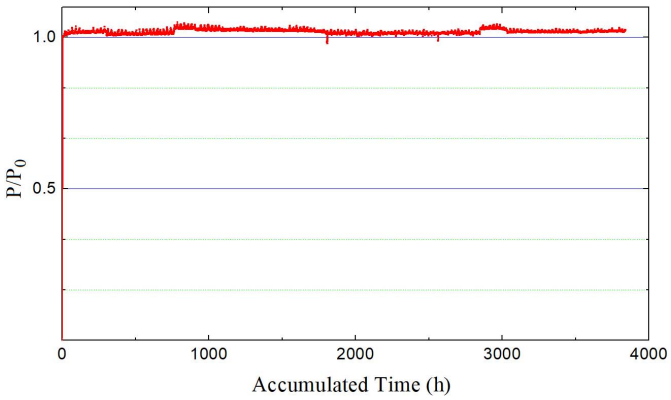

Fig. 4. Lifetime test with one single emitter under CW 12 A bias and 40°C.

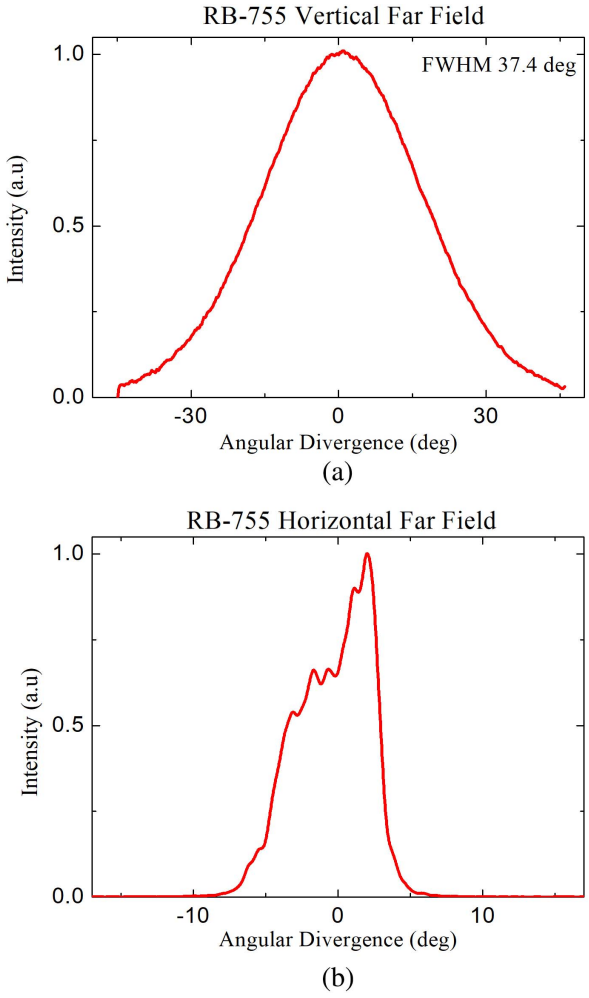

Fig. 5. (a) Vertical (fast axis) far-field angular divergence. (b) Horizontal (slow axis) far-field angular divergence.

and the slope efficiency η can also be defined similarly,

$$\eta(T) = \eta_0 \cdot \exp\left(\frac{T_1 - T}{T_1}\right), \tag{3}$$

where the parameters T_0 and T_1 are the characteristic temperature. By taking the natural logarithm on both sides of Eqs. (2) and (3), we can write the natural logarithm of the threshold and slope efficiency as functions of the absolute temperature with the first derivative being the inverse of characteristic temperature. The results are shown in Fig. 6, and data points are fitted with a line. T_0 and T_1 are extracted as 139.5 and 440.5 K, respectively, which are better than those reported in the literature[7]. We believe the reason for the better performance of our device is the higher Al content (15% in RB-755, 10% in Ref. [7]) in our waveguide layer, which leads to a higher energy barrier around the QW and eventually higher quantum efficiency under high temperature.

There are certain features that make our device distinguished. It should be noted that the bilayer waveguide

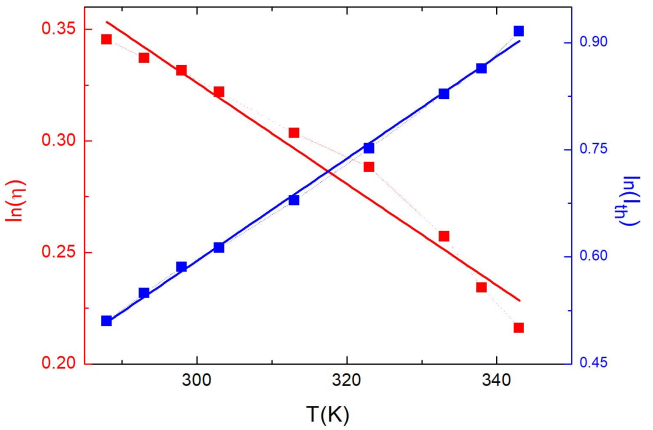

Fig. 6. Measured natural logarithm of threshold and slope efficiency as functions of absolute temperature. The slope of fitted lines corresponds to the inverse of T_0 (blue) and T_1 (red), respectively.

structure described above adds up to a large optical cavity around 1.4 μm in thickness. Also, a ridge-etching process is employed during fabrication to provide a lateral gain guiding mechanism, forming a large current aperture of 350 μm width. The Fabry–Pérot cavity length is 2.5 mm, which is longer than most other products designed for operation in this wavelength range. In spite of the fact that threshold current is relatively large as one of the results, the large size of the optical cavity is supposed to effectively lower the energy density inside the device and better suppress waveguide loss. A large emitting width can hold power density at the facet on a low level, which significantly increases the total output power free from facet COD.

With a threshold of 2 A, 1.27 W/A slope efficiency, and high COD power, our devices are capable of providing a world-leading 12.7 W output highly monochromatic laser in the CW operation mode at a wall-plug efficiency of over 54%. Meanwhile, the lifetime extending over 3800 h demonstrates extraordinary reliability.

This work was supported by the National Key R&D Program of China (No. 2016YFB0401802) and the Project of Committee for Science and Technology Innovation of Shenzhen (No. JSGG20160301095954267).

References

1. J. Royo, J. Moreno-Moraga, and M. A. Trelles, Lasers Surg. Med. **49**, 355 (2017).
2. N. Van Geel, L. Depaepe, and R. Speeckaert, J. Eur. Acad. Dermatol. Venereol. **29**, 1121 (2015).
3. P. L. Tihanyi, F. C. Jain, M. J. Robinson, J. E. Dixon, J. E. Williams, K. Meehan, M. S. O'Neill, L. S. Heath, and D. M. Beyea, IEEE Photon. Technol. Lett. **6**, 775 (1994).
4. M. A. Emanuel, J. A. Skidmore, M. Janson, and R. Nabiev, IEEE Photon. Lett. **9**, 1451 (1979).
5. A. Knauer, G. Erbert, H. Wenzel, A. Bhattacharya, F. Bugge, J. Maege, W. Pittroff, and J. Sebastian, Electron. Lett. **35**, 638 (2002).

6. G. Erbert, F. Bugge, A. Knauer, J. Sebastian, A. Thies, H. Wenzel, M. Weyers, and G. Trankle, IEEE J. Sel. Top. Quantum Electron. **5**, 780 (1999).
7. A. Al-Muhanna, J. K. Wade, T. Earles, and L. J. Mawst, Appl. Phys. Lett. **73**, 2869 (1998).
8. D. P. Bour, D. W. Treat, K. J. Beernink, R. L. Thornton, T. L. Paoli, and R. D. Bringans, IEEE Photon. Lett. **6**, 1283 (1994).
9. E. Nomoto, T. Taniguchi, T. Ohtoshi, T. Funane, K. Saito, and S. Sasaki, in *International Conference on Indium Phosphide and Related Materials*, IEEE (2008), p. 1.
10. G. I. Hatakoshi, K. Itaya, M. Ishikawa, M. Okajima, and Y. Uematsu, IEEE J. Quantum Electron. **27**, 1476 (1991).
11. V. Rossin, M. Peters, E. Zucker, and B. Acklin, Proc. SPIE **6104**, 610407 (2006).